PCCP

PAPER

View Article Online
View Journal | View Issue

Cite this: *Phys. Chem. Chem. Phys.*, 2016, **18**, 1140

Mechanisms of low temperature capture and regeneration of CO_2 using diamino protic ionic liquids†

Tristan J. Simons,*[ab] Thomas Verheyen,[a] Ekaterina I. Izgorodina,*[a] R. Vijayaraghavan,[a] Scott Young,[a] Andrew K. Pearson,[ab] Steven J. Pas[ab] and Douglas R. MacFarlane[a]

Received 31st August 2015,
Accepted 30th November 2015

DOI: 10.1039/c5cp05200a

www.rsc.org/pccp

Carbon dioxide (CO_2) chemical absorption and regeneration was investigated in two diamino carboxylate protic ionic liquids (PILs), dimethylethylenediamine formate (DMEDAH formate) and dimethylpropylenediamine acetate (DMPDAH acetate), using novel calorimetric techniques. The PILs under study have previously been shown to possess a CO_2 absorption capacity similar to the industrial standard, 30% aqueous MEA, while requiring much lower temperatures to release the captured CO_2. We show that this is in part due to the fact that the PILs exhibit enthalpies of CO_2 desorption as low as 40 kJ mol^{-1}, significantly lower than the 85 kJ mol^{-1} required for 30% aqueous MEA. Computational and spectroscopic analyses were used to probe the mechanism of CO_2 capture, which was found to proceed *via* the formation of carbamate moieties on the primary amine of both DMEDAH and DMPDAH. Evidence was also found that weakly acidic counter-ions such as formate and acetate provide, unexpectedly, an additional proton acceptor site in the traditional carbamate mechanism, revealing opportunities to increase CO_2 uptake capacity in the future through careful design of the anion and cation used in the PIL capture agent.

1 Introduction

Due to the increasing amounts of greenhouse gases entering the atmosphere from human activity, the efficient capture of CO_2 has been proposed as a possible mechanism by which climate change may be slowed or even reversed.[1] Most reasonably, the focus of these agents have been centered on capturing CO_2 at the most concentrated anthropogenic sources, such as flue gas streams of coal-fired power stations.[2,3] While such large-scale applications have received the majority of the research focus in the CO_2 capture field, there exist many applications in which CO_2 must be sequestered and regenerated from less concentrated and hostile environments. Many of these environments possess atmospheres that do not contain high concentrations of CO_2 that are needed to drive the chemical and physical capture equilibria forward. One such application is the removal of CO_2 from occupied, hermetically sealed environments where the accumulation of CO_2 may become toxic to the inhabitants (*e.g.* space shuttles). Prolonged exposure to elevated levels of CO_2 can lead to a number of health issues,[4] thus the importance of safe and efficient CO_2 capture over a range of applications cannot be overstated.

Room temperature ionic liquids (RTILs) are a unique class of chemical solvents in that they are composed of organic anions and cations that remain liquid at room temperature.[5] The resulting liquid is often viscous, but is both conductive and is usually of low volatility due to being composed entirely of charged species – much like a molten salt. The number of possible RTILs has been calculated to be extremely high, due to the countless chemical moieties that can be incorporated into the cation and anion structure, providing an enormous range of possible physical, chemical and electrochemical properties. One subset of RTILs are protic ionic liquids (PILs), which are synthesized by a proton transfer reaction between a Brønsted acid and a Brønsted base. This proton transfer reaction can be incomplete, depending on acidity/basicity of the acid and base respectively; this results in an equilibrium between the charged and neutral forms of each species.

Several studies have probed the degree of proton transfer and the resulting physiochemical properties of PILs through an analysis of the difference in pK_a^{aq} values (ΔpK_a^{aq}) of the starting acid and base materials. Stoimenovski *et al.*,[6] Yoshizawa *et al.*[7] and Miran *et al.*[8] all established a clear relationship between a

[a] *School of Chemistry, Monash University, 17 Rainforest Walk, Clayton 3800, Australia. E-mail: Tristan.simons@monash.edu, katya.pas@monash.edu*
[b] *Maritime Division, Defence Science & Technology Group, Department of Defence, Fishermans Bend 3207, Australia*

† Electronic supplementary information (ESI) available. See DOI: 10.1039/c5cp05200a

higher ΔpK_a value and the physiochemical properties more closely associated with traditional aprotic RTILs – such as high thermal stability and low volatility – caused by a more complete proton transfer reaction. Conversely, a lower ΔpK_a^{aq} value led to behavior more closely related to the uncharged starting materials. The studies concluded that in order to attain the unique properties of RTILs in a PIL, a ΔpK_a^{aq} value as high as possible is desirable. It was also found that the presence of other functional groups that provided an H-bonding environment favoured the formation of the ionic species. Thus ΔpK_a^{aq} is a qualitatively useful parameter by which the physical and chemical properties of PILs can be tuned when designing PILs for specific tasks – such as CO_2 absorption. However, it was also clear in these prior studies of protic equilibria in PILs that the extent of proton transfer was lower than expected on the basis of the aqueous data, in other words ΔpK_a^{IL} can be considerably smaller than ΔpK_a^{aq}.

In general, CO_2 capture agents fall into two broad categories; those that capture CO_2 through physical mechanisms and those that capture by chemical mechanisms. Physical CO_2 capture agents (such as metal organic frameworks,[9] unfunctionalised RTILs[10] and carbon fibres[11]) rely on high concentrations of ambient CO_2 to partake in weak intermolecular interactions that hold the CO_2 in the material as long as the CO_2 partial pressure is maintained. Upon relief of the high CO_2 partial pressure, these materials will surrender the physically adsorbed CO_2, at which time it can be compressed or released. While physical adsorbents require high partial pressures of CO_2 to be effective, chemical absorbents form covalent bonds between the absorbent and the CO_2 molecule and can do so at relatively lower partial pressures. These capture reactions tend to be exothermic, meaning that the CO_2 regeneration process requires a greater input of energy, hence requiring elevated temperatures. This in turn can lead to several complications that reduce the efficiency of a CO_2 capture agent such as thermal breakdown and solvent loss due to increased volatility.[12]

Probably the most common group of chemically absorbent materials used in CO_2 scrubbing are those that are based on amine (NH_2) functionalities, such as in monoethanolamine (MEA) or amine functionalized RTILs. The covalent addition of CO_2 to the NH_2 moiety of the amine is known as the carbamate formation mechanism (Scheme 1).

When CO_2 is chemically captured, it is covalently bound to the amine to form a carbamate functionality. The addition causes the loss of a proton due to the high acidity of the newly formed molecule, which is accepted by a second molecule of the amine, thus forming an ion pair. The unfortunate consequence of the capture agent also being the strongest available proton acceptor results in a theoretical limitation to the amount of CO_2 captured, $n(CO_2)/n(\text{amine}) = 0.5$.

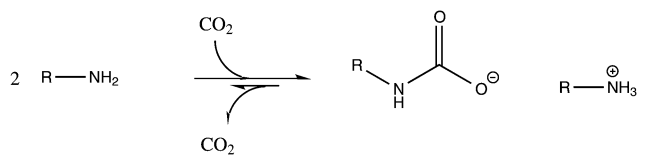

Scheme 1 The carbamate formation mechanism of CO_2 capture.

The low volatility and potentially reduced corrosion properties make ILs that contain a primary amine functionality a valuable target for investigation as a chemical CO_2 capture absorbent. Seo *et al.*[13] investigated a series of aprotic imidazolium-based cations paired with aprotic heterocyclic amine anions. In addition to the novelty of using the anion as the site of carbamate formation, it was found that the presence of the imidazolium cation facilitated the establishment of two separate capture mechanisms. At lower partial pressures of CO_2 (<0.1 bar), the heterocyclic amine captured the CO_2 *via* carbamate formation. As the partial pressure was increased, the CO_2 was also captured at the C2 position of the imidazolium cation *via* a carbene intermediate formed by a deprotonation reaction. By way of this dual-mechanism, ratios of CO_2 uptake well above 0.5 were obtained at CO_2 partial pressures below 1 bar. One drawback of this work was that, like many large RTIL/PIL capture species which can achieve high molar CO_2 capture ratios, the high molecular weight of the ions (*e.g.* $[P_{6,6,6,14}][4\text{-triaz}] = 551.93$ g mol^{-1}) results in a relatively low volumetric or gravimetric CO_2 absorption capacity. Niedermaier *et al.*[14] have also shown that different CO_2 capture mechanisms can be possible at different partial pressures of CO_2 in taurinate based PILs. It was discovered that at low pressures, the traditional carbamate mechanism was prevalent, however as the pressure was increased, carbamic acid formation was stabilized such that more than 0.5 mol of CO_2 per mole of PIL could be absorbed.

Vijayaraghavan *et al.*[15] investigated a series of PILs based on diamine based mono-cations paired with various carboxylate, triflate and halide counter anions. The carboxylate PILs studied were shown to facilitate the formation of carbamate at the primary amine at ratios approaching 0.4 at room temperature and 1 atm CO_2. Of particular note was the relatively low temperature at which the CO_2 was released (approximately 40 °C). The relatively low molecular weight of the PILs used in the study produced specific capacities (g_{CO_2}/g_{PIL}) that were comparable to the current industry standard, 30% aqueous solution of MEA. In the present report, we further investigate two of the candidate PILs initially studied by Vijayaraghavan *et al.* – dimethylethylenediamine formate (DMEDAH formate) and dimethylpropylenediamine acetate (DMPDAH acetate) to gain a deeper understanding of the observed behavior and mechanism of action in diamine PIL CO_2 absorbers, in particular the low desorption temperatures.

2 Experimental methods

2.1 Materials

N,*N*-Dimethylethylene diamine (DMEDA, 99%, Sigma), (3-dimethylamino)-1-propylamine (DMPDA, 99%, Sigma), formic acid (99.9%, Sigma) and acetic acid (99.9% Sigma) were used as received.

2.2 Synthetic methods

DMEDAH formate (*N*,*N*-dimethylethylenediammonium formate, Fig. 1a) and DMPDAH acetate ((3-dimethylamino)-1-propylammonium acetate, Fig. 1b) and DMPDAH NTf_2 ((3-dimethylamino)-1-propylammonium bis(trifluoromethanesulfonyl)imide) were synthesised according to literature methods described

previously.[15] Full experimental details including NMR assignments are described in the ESI.† Water content was established to be less than 1% (w/w) on a Metrohm Model 756 Karl Fischer Coulometer using Hydranal Coulomat AG titrant.

2.3 Viscosity

Viscosity measurements were performed on an Anton Paar Lovis 2000M falling ball viscometer. The sample was inserted into a 2.5 mm glass capillary with a 1.5 mm stainless steel ball of density 7.69 g cm^{-3} and performed at 25 °C at an angle of 60°.

2.4 Density

Density measurements were performed on an Anton Paar DMA5000 Density Meter which operates using the oscillating U bend method. The instrument was equilibrated at 25 °C for 15 minutes prior to the measurement being taken.

2.5 Differential scanning calorimetry (DSC)

The temperature at which CO_2 is released from the PIL was determined by weighing out approximately 15 mg of each PIL and placing in an aluminium DSC pan. To allow for the exchange of gases into and out of the liquid, the pans were kept open (unsealed). The sample was then set in the TA Q100 DSC, and cooled from 40 to 20 °C. This temperature was chosen because these PILs have been demonstrated to absorb CO_2 at room temperature.[15] Once equilibrated, the flow gas was changed from pure N_2 to pure CO_2 (>99.9%, 50 mL min^{-1}), resulting in absorption by the sample. This was continued for 60 minutes until the sample was effectively saturated with CO_2. The flow gas was then reverted back to N_2, and the sample heated at a rate of 2 °C per minute to 80 °C. The DSC was separately calibrated using a standard of sapphire under the same heating and gas flow.

To investigate the PILs ability to perform multiple CO_2 loading and stripping cycles under DSC conditions, samples were prepared and cooled to 20 °C in the same way. Because the sample would need to be heated to induce unloading, a baseline temperature jump to 40 °C was performed and maintained for 60 minutes. The sample was then cooled back to 20 °C and exposed to CO_2 for 60 minutes before the flow gas was reverted to N_2 and the temperature stepped back to 40 °C (for 60 minutes). This process of performing a baseline, absorption and desorption processes was then repeated twice or more. The baseline was determined before each cycle due to the possibility of a small amount of sample mass loss; however consistent energy results were obtained when it was established on each cycle. This mass loss can also be seen by the slight reduction in the absorption peak from one cycle to the next, caused by the decrease in available amine for carbamate formation.

To determine the enthalpy of desorption, the 15 mg samples were loaded with CO_2 in a sample jar with a ~1 g pellet of dry ice. The jar was loosely closed for the first 30 minutes while the CO_2 sublimed and reached room temperature, then closed for 60 minutes to ensure equilibrium absorption conditions were reached with ~1 atm of CO_2. This method of loading was used to minimize the sample loss associated with loading under a stream of CO_2 in the DSC. The sample was then weighed, placed in the DSC to record the desorption endotherm. A blank run of each PIL was also performed to allow a baseline subtraction.

2.6 Attenuated total reflectance infra-red (ATR-IR)

All ATR-IR liquid experiments were performed on a Bruker Equinox 55 FTIR, fitted with a Specac ATR Unit fitted with a diamond crystal. Data were collected on the OPUS software provided with the instrument. All samples were run at a resolution of 2 cm^{-1}, averaging 128 scans in the range of 600 cm^{-1} to 4000 cm^{-1} at 20 °C in an open atmosphere.

2.7 Computational methods

All quantum chemical calculations were performed using the GAUSSIAN09 package.[16] All geometry optimizations were performed at M062X[17]/aug-cc-pVDZ[18] level of theory. The M062X functional of the Minnessota family was shown to perform reliably for studying energetics of ion pairs in ionic liquids.[19] The conductor-like polarizable continuum model (CPCM)[20] was used to account for the stabilizing effect of surrounding ions, with water being used as a solvent. This combination was successfully used for the prediction of crystal structures of methanide-based ionic liquids.[21] The DMEDA amine was fully conformationally screened at the same level of theory. The protonated versions of the DMEDA amine were obtained by placing the proton at either primary or tertiary amine centre. Improved electronic energies were obtained at the M062X/aug-cc-pVTZ[18] level of theory. These improved energies were also corrected by zero-point vibrational energy (ZPVE) from M062X/aug-cc-pVDZ geometry optimizations as discussed above. Further in the text these improved energies are referred to as total electronic energies.

3 Results and discussion

3.1 Loading and regeneration of CO_2 in PILs

Table 1 presents the physical properties of the PILs in their neat and loaded states; it also includes DMPDAH NTf_2 and 30% aqueous MEA literature data for comparison. The CO_2 loading method used here is similar to the work of Vijayaraghavan[15] but utilizes a smaller sample size and thus is much less impacted by the rising viscosity of the samples during loading. This is particularly significant for the DMPDAH acetate sample, for which we report a higher loading than in the previous report.

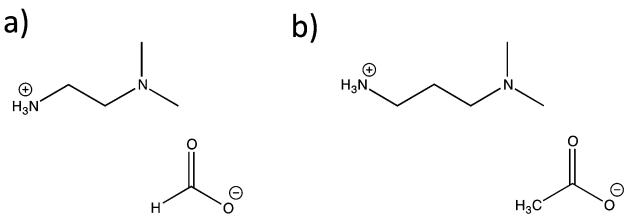

Fig. 1 Chemical structure of (a) DMEDAH formate and (b) DMPDAH acetate.

Table 1 Enthalpy of CO_2 absorption, CO_2 capacity and physical properties of DMEDAH formate, DMPDAH acetate, DMPDAH NTf_2 and 30% aqueous MEA solution. A full discussion of the calculation of ΔH is located in the Experimental methods section

Sample	Density (25 °C)/ (g cm^{-3}) ± 5 × 10^{-5}		Viscosity (25 °C)/ (mPa s) ± 5		CO_2 absorption capacity (% g g^{-1}) ± 1	CO_2 absorption capacity (% g cm^{-3}) ± 1	Mole ratio/(n(CO_2)/ n(amine)) ± 0.05	$\Delta H^{desor}_{CO_2}$/ (kJ mol^{-1}) ± 5
	Pure	+CO_2	Pure	+CO_2				
DMEDAH formate	1.02273	1.07045	186	491	11.8	12.7	0.36	40
DMPDAH acetate	0.97071	1.01046	1110	1043 (35 °C)	15.6	15.8	0.58	50
DMPDAH NTf_2	1.47991	—	—	—	1.7	2.5	0.14	60
30% MEA in H_2O	—	—	—	—	13.1	13.2	0.61	85[22]

DMEDAH formate shows a CO_2 capacity of 11.8% (g g^{-1}), only slightly below the MEA solution at 13.1% (g g^{-1}). When this is considered volumetrically, it equates to 12.7% (g cm^{-3}) compared to 13.2% (g cm^{-3}) for the MEA solution. In contrast, DMPDAH acetate appears to outperform both DMEDAH formate and the MEA solution, showing a capacity of 15.6% (g g^{-1}) and 15.8% (g cm^{-3}). One of the further advantages of these diamino PILs is that they are less basic than MEA, meaning that the dilute solutions that prevent high rates of corrosion can be avoided. This in turn increases the CO_2 capture site density in the PIL compared to the 30% MEA solution, providing the comparable capacities shown in Table 1.

It would initially appear counter-intuitive to suppose that the PIL with the higher atomic weight (and similar density) DMPDAH acetate could possess a CO_2 capacity significantly higher than the lighter DMEDAH formate. The mole ratio of free amine to CO_2 captured for DMEDAH formate was calculated to be 0.36 at 1 atm CO_2 (Table 1), appreciably lower than the established 0.5 ratio carbamate limit (Scheme 1). However, DMPDAH acetate appears to exceed the 0.5 theoretical limit, showing a ratio of 0.58 in the neat state. Evidently, there are complexities in the mechanism that mean the traditional carbamate mechanism is not sufficient to explain this observed behavior, as will be discussed further below.

Viscosity and density were measured for both DMEDAH formate and DMPDAH acetate, before and after loading, as shown in Table 1. In the neat state, DMPDAH acetate shows a viscosity higher than DMEDAH formate (1110 mPa s and 186 mPa s respectively). As expected, the viscosity increases significantly upon absorption of CO_2, with DMEDAH formate climbing to 491 mPa s^{-1} and the DMPDAH acetate becoming so viscous that measurements could not be performed at 25 °C in the apparatus used. While these increases are indicative of the carbamate formation mechanism with excellent CO_2 capacity, the highly viscous nature of these liquids reduces the kinetics of CO_2 absorption and regeneration. This issue may be overcome through the addition of H_2O or other such polar solvents, which has the effect of lowering the viscosity of the resulting solution.[23,24] This investigation is currently under way in our laboratories.

A key finding of the work by Vijayaraghavan[15] was that some diamino PILs utilizing carboxylate anions could absorb CO_2 at room temperature and release it again at only slightly elevated temperatures (approximately 40 °C). The origin of this low desorption temperature may in part be due to a significantly lower enthalpy of CO_2 desorption. To establish the enthalpy of CO_2 desorption $\left(\Delta H^{desor}_{CO_2}\right)$, the difference in observed heat flow in the DSC between a loaded and unloaded PIL sample was combined with the observed mass change during a temperature step to 40 °C (Fig. 2). Because of the relatively slow kinetics of desorption it was found that isothermal T-step DSC experiments more successfully displayed the desorption exotherm than scanning runs. To the authors' knowledge, this is among the first published results demonstrating the calculation of CO_2 desorption enthalpies using DSC techniques.

It can be clearly seen for both DMEDAH formate (Fig. 2a) and DMPDAH acetate (Fig. 2b), that when the PIL is in the neat state, a temperature step endotherm appears (blue curves), after which the baseline is re-established after a period of time. In the case of the neat DMEDAH formate and to a far lesser extent DMPDAH acetate, the main endotherm is preceded by a small exotherm that is not observed in the CO_2 loaded cases. As no exothermic feature is seen in this region in the scanning DSC experiment, this feature is attributed to an instrumental artifact caused by the rapid temperature change experienced by the neat PIL in this part of the experiment. Why this should not occur in the CO_2 loaded samples is yet to be determined.

A more pronounced endotherm is observed in the case of the CO_2 loaded sample. By calculating the difference in heat flow of this peak, the effective enthalpy of this CO_2 desorption process can be estimated. This observed endotherm appears due to the difference in heat capacity between the sample and the reference side of the instrument and the effect this has during the very rapid temperature step. We note that the enthalpy change in this experiment includes a small heat capacity difference component, which is nonetheless a real component of the energy requirements of a practical system.

Table 1 shows the enthalpy data as well as the calculated CO_2 capacity for each PIL. For comparison, the industry standard, literature data 30% aqueous MEA is also shown. DMEDAH formate and DMPDAH acetate show $\Delta H^{desor}_{CO_2}$ of 40 ± 5 kJ mol^{-1} and 50 ± 5 kJ mol^{-1} respectively, far below the 85 kJ mol^{-1} seen in the MEA standard. For comparison data is also listed for DMPDAH NTf_2 and literature data for 30% MEA in H_2O. The result for DMEDAH formate is reasonably consistent with that (46 kJ mol^{-1}) estimated from the pressure/temperature data presented by Mumford *et al.*[25] for this compound.

To investigate the ability of the PILs to undergo numerous absorption/regeneration cycles, a novel DSC technique involving

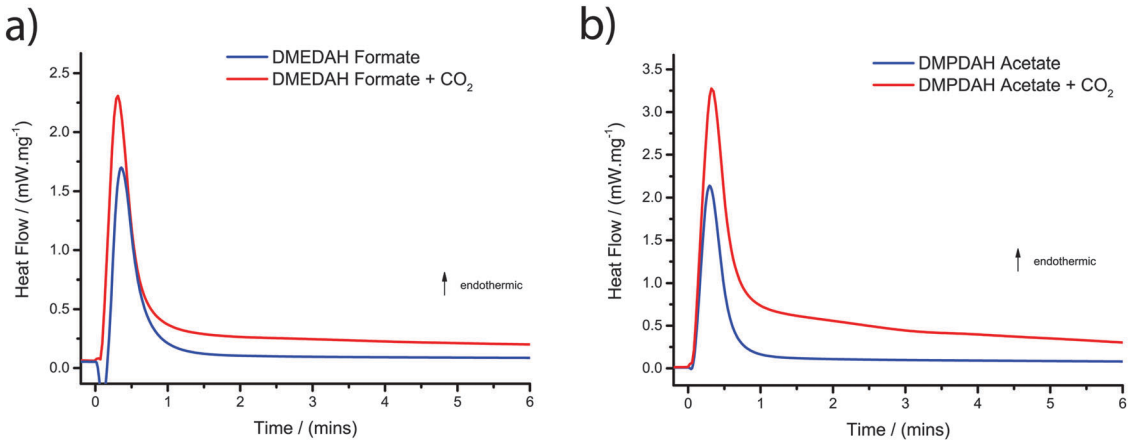

Fig. 2 DSC traces of the isothermal (40 °C) CO_2 desorption for (a) DMEDAH formate and (b) DMPDAH acetate after a temperature step from 20 °C.

a number of gas streams and temperature steps was utilised (Fig. 3).

In these cycling experiments, the sample was inserted at 20 °C and stepped to 40 °C under N_2 in order to establish the baseline of the PIL sample when no CO_2 was present. The sample was then cooled rapidly to 20 °C at which time the gas stream was switched to CO_2 for the absorption process, which manifests itself as a clear exotherm. Once the PIL was loaded with CO_2 for 60 min, the temperature was once again stepped to 40 °C and the gas stream switched back to N_2 to perform desorption of the CO_2. This cycle then repeats; Fig. 3 shows the detail of two cycles. For comparison, a study of 30% MEA aqueous solution was attempted using this technique; however the extreme volatility of this solution caused it to evaporate under these conditions before a single cycle could be completed. Thus these DSC results demonstrate the feasibility of a PIL based CO_2 absorber that undergoes numerous absorption/regeneration cycles at low regeneration temperature. The slight volatility observed could be dealt with by using an activated carbon scrubber in the absorber system.

3.2 Speciation and mechanism

Due to the presence of the diamine cation in the PILs under study, the carbamate formation reaction likely involves a complex series of equilibria as illustrated in Scheme 2.

Each section of the mechanism (1, 2 and 3) and the associated experimental and theoretical data will be discussed individually in the following sections.

3.2.1 Speciation of the PIL. The native PIL structure that is assumed to make up the majority of ionized species consists of a DMEDAH cation with the positive charge on the primary amine (**a**) and the formate anion with a delocalized negative charge over the two oxygen atoms (**b**). It is well established that the degree of proton transfer in PILs is related to the relative difference in acidity/basicity of the starting materials, or the ΔpK_a^{aq}.[6] In the case of the two diamine carboxylates under study, the ΔpK_a calculated on the basis of the higher pK_a of the two amine groups in the diamine, is around 6 which would normally be sufficient to indicate a strong degree of proton transfer. As well as this equilibrium, it is also possible for the acidic proton on the primary amine to exchange to the slightly

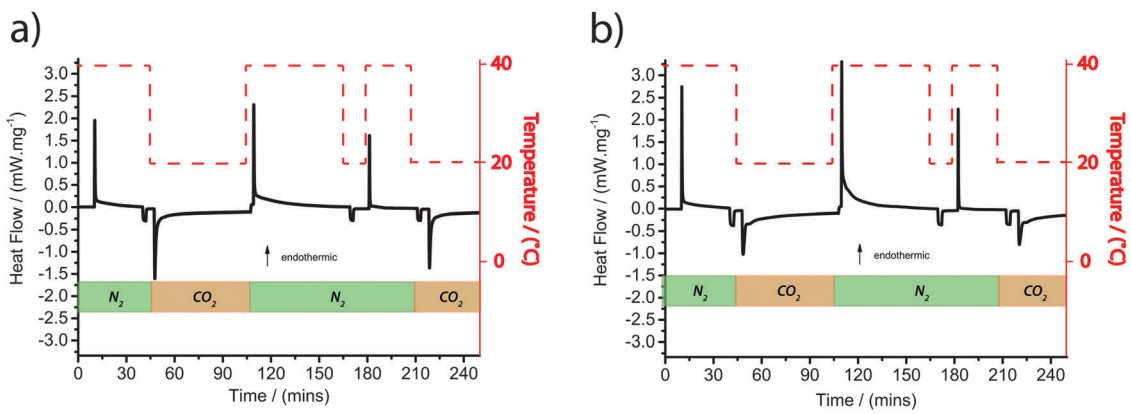

Fig. 3 DSC traces of the CO_2 absorption/regeneration cycles of (a) DMEDAH formate and (b) DMPDAH acetate. Temperature steps undertaken in 1 atm of flowing N_2 gas are shown in green, while those under 1 atm flowing CO_2 are in orange.

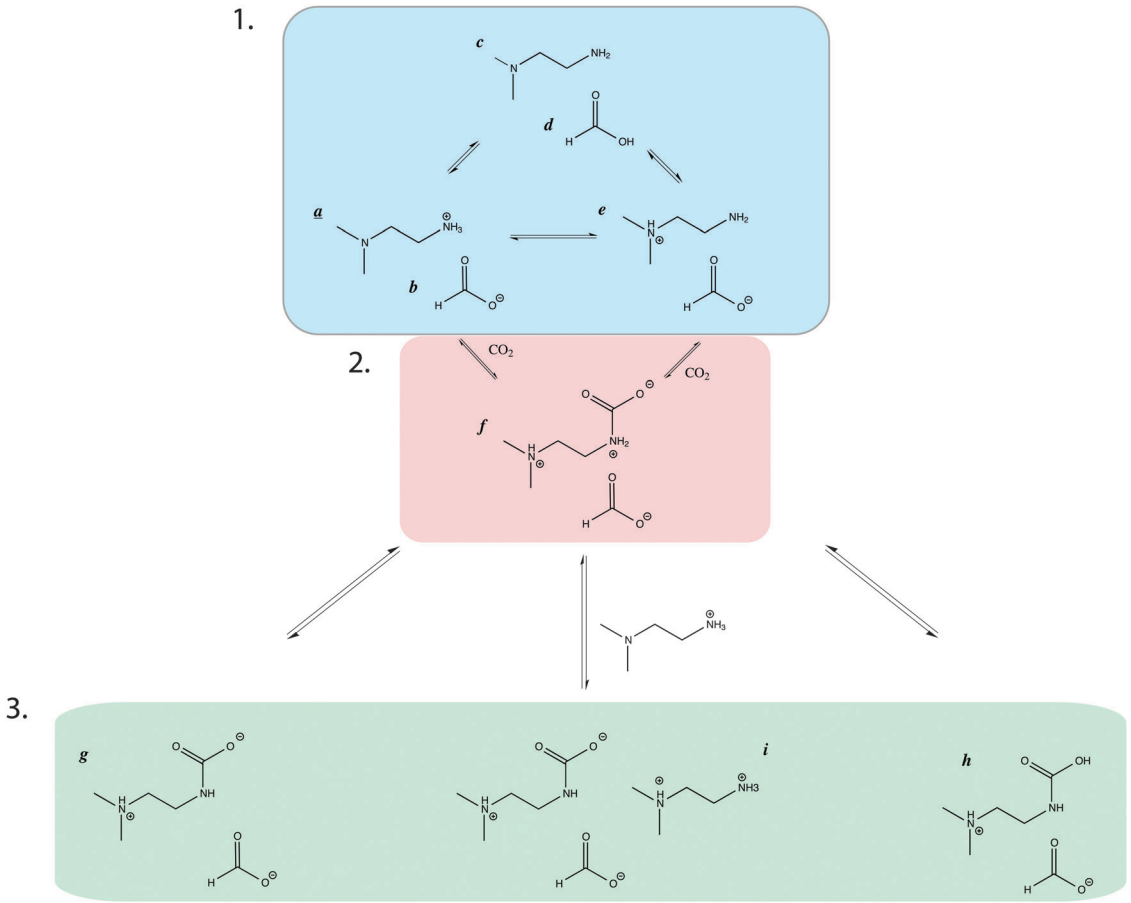

Scheme 2 Possible reaction pathways for the capture of CO_2 in DMEDAH formate by the carbamate formation mechanism. (a–i) Indicate the range of different individual ions that are possible for ease of identification.

less basic tertiary amine. As such, it can be expected that both of these species will be present at equilibrium.

To probe this concept, *ab initio* geometry optimization of two plausible clusters was performed. Both clusters consisted of two cations and two anions. One cluster had the DMEDA amine protonated in the primary centre (**a**), and in the other the tertiary centre (**e**). DMEDAH formate clusters were used for the comparison to DMEDAH formate experimental data, but in order to reduce the computational cost of these calculations, DMEDAH acetate was investigated for comparison to DMPDAH acetate experimental data. The similarity in the structures and active sites was considered sufficient for the comparison to be valuable. 3D representations of all clusters modelled can be found in Fig. S3 and S4 (ESI†).

Fig. 4 shows FTIR spectra of the pure DMEDAH formate along with the calculated theoretical band positions to probe whether the protonation primarily occurred on the primary (**a**) or tertiary (**e**) amine. Since it is well known that theoretical spectra overestimate experimentally observed bands (especially stretching vibrations[26]), the predicted IR spectra were scaled to reproduce the C–H stretching in the formate anion observed at 2773 cm^{-1} in the experimental data (Fig. 4 (top)). The C–H stretch was selected as it displayed a distinct sharp peak in the experiment. It has to be noted that all vibrational frequencies were scaled using the same scaling factor for each cluster.

In Fig. 4 (bottom), the calculated spectra for clusters having the DMEDAH protonated at the tertiary or primary centers are shown in magenta and black, respectively. Fig. 4 (top) is the experimental spectrum of the neat DMEDAH formate. Key peaks present in the experimental data that appear from the calculated data to be indicative of the protonated tertiary amine cluster are located in the C–H region at 2985 cm^{-1}, as well as the C–O stretch at 1357 cm^{-1} which appears as a small peak. Conversely, clear peaks associated with the protonated primary amine include the strong C–H band at 2528 cm^{-1} as well as the C–O stretch at 1511 cm^{-1}. The presence of both sets of distinctive peaks supports the fact that both amine groups are protonated to some observable equilibrium extent.

This same methodology was also applied to DMPDAH acetate (Fig. 5) which shows a similar relationship between the calculated and the experimental spectra. In this case, the C–C stretch observed at 1393 cm^{-1} was selected as the reference to scale the theoretical spectra.

Once again, a combination of the primary protonated and tertiary protonated clusters reproduces the experimentally observed spectrum. A broad peak at 1540 cm^{-1} corresponding to the asymmetric COO– vibration correlates well with the

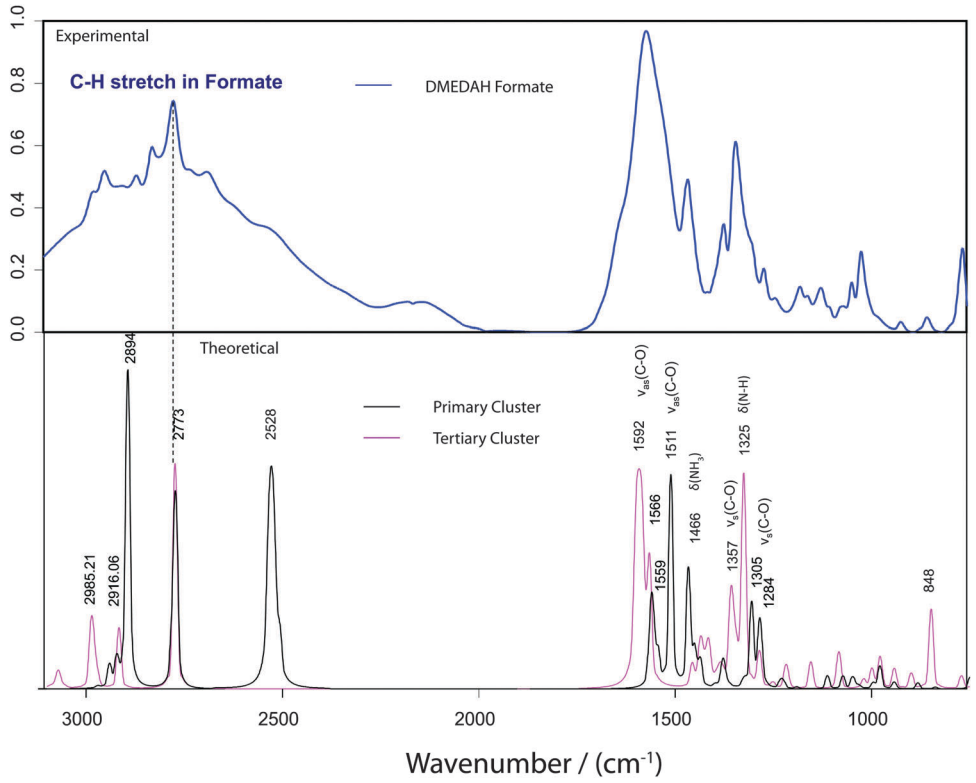

Fig. 4 Bottom: calculated FTIR spectra of DMEDAH formate primary amine protonated cluster (black) and tertiary amine protonated (magenta). Normalized to the C–H Stretch of formate. Top: experimental ATR-IR of DMEDAH formate. Both spectra have been normalized to the C–H in formate at 2773 cm^{-1}. A scaling factor of 0.933 and 0.961 were used for the primary and tertiary protonated clusters respectively.

peaks at 1515 and 1545 cm^{-1} in the protonated primary amine cluster and a broad peak at 1555 cm^{-1} in the tertiary case. The NH_3 deformation at 1599 cm^{-1} observed in the former corresponds to the shoulder developing at 1600 cm^{-1} in the experimental spectrum, whereas the N–H bending vibration at 1327 cm^{-1} correlates with a moderate peak at 1389 cm^{-1}. From this data it can be concluded that both mono-protonated forms (primary and tertiary protonation) of DMPDAH are present in this PIL.

3.2.2 Formation of the carbamate. In order to confirm the expectation that the tertiary amine group is not the site of CO_2 addition, several tertiary diamine carboxylates were tested for their ability to chemically absorb CO_2. PILs based on *N*,*N*,*N*′,*N*′-tetramethylethylenediamine (TMEDA) were synthesized, however the PILs based on both formate and acetate were found not to form a homogenous liquid due to poor proton transfer. However, the PIL based on triflate (OTf) was found to form a homogenous PIL, TMEDAH OTf. In this PIL, bearing two tertiary amines, CO_2 uptake was found to be extremely poor, showing no spectroscopic evidence for chemical absorption. This demonstrates that carbamate formation on a tertiary amine is very energetically unfavorable due to the necessary formation of a permanent zwitterion at the tertiary nitrogen. As such, it appears that carbamate formation must occur exclusively on the primary amine in both DMEDAH and DMPDAH. As the formation of carbamate occurs through a nucleophilic addition of CO_2 to the terminal nitrogen of the primary amine, CO_2 capture can only occur when the primary amine remains unprotonated – leaving the nitrogen lone pair free to attack the CO_2. As such, the ability of the proton to freely exchange between the tertiary (**e**) and primary (**a**) amine is a key requirement in the formation of the carbamate zwitterion (**f**).

Our previous work[27] explored whether interaction between CO_2 and a series of IL ions caused any change in its geometry (*i.e.* bending) or charge transfer. We found only slight differences in the strength of interaction as the interaction was in general rather weak.

3.2.3 Speciation in the loaded state. Interestingly, the mechanism by which the primary ammonium proton can be transferred to the tertiary centre appears to be dependent on the PIL anion. Experiments utilizing a much stronger acid as the source of the counter anion show that this eliminates nearly all of the CO_2 uptake capacity. For example, by using bis-(trifluoromethanesulfonyl)imide (NTf_2) anion instead of the carboxylates, the molar CO_2 uptake was greatly diminished (Table 1). This suggests that reformation of the weak acid is a key intermediate step in the transfer of the proton from the primary to the tertiary amine in both DMEDAH and DMPDAH. When a strong acid is present, the proton is less readily transferred back to the anion (**d**) in the intermediate step, preventing the formation of the neutral primary amine to undergo CO_2 addition. It should also be noted that it is also possible for CO_2 to add to the intermediate neutral diamine molecule (**c**) generated in this intermediate state.

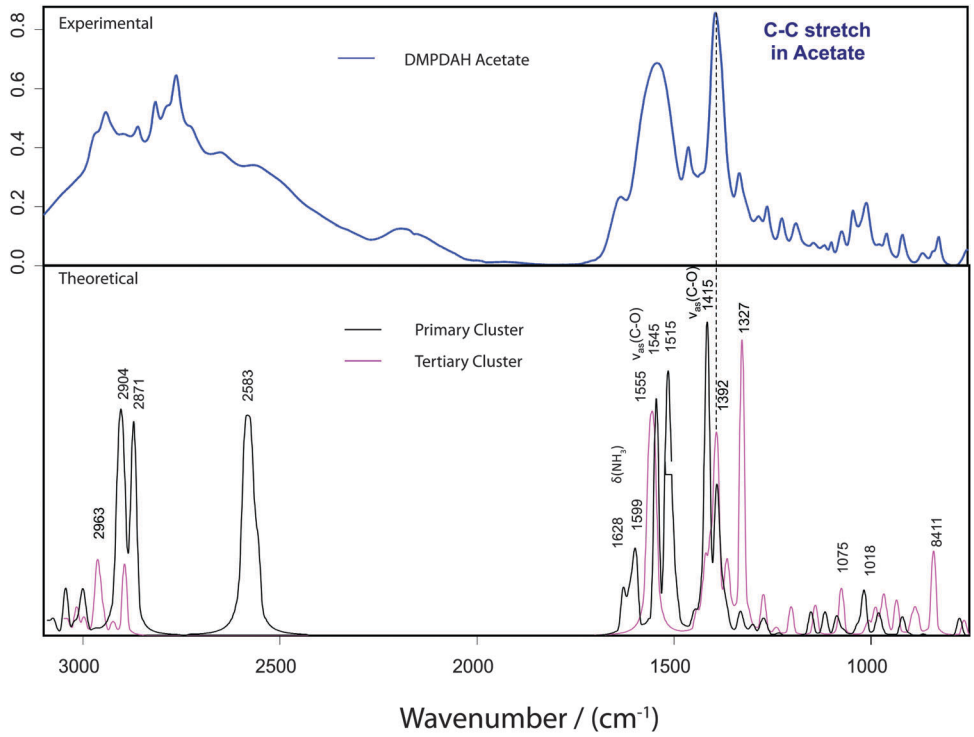

Fig. 5 Bottom: calculated FTIR spectra of DMEDAH acetate primary amine protonated cluster (black) and tertiary amine protonated (magenta). Top: experimental ATR-IR spectra of DMPDAH acetate. Both spectra have been normalized to the C–C stretch in acetate at 1392 cm^{-1}. A scaling factor of 0.966 and 0.963 were used for the primary and tertiary protonated clusters respectively.

Thus the addition of CO_2 must occur at the primary amine of a diamine cation that is protonated at the tertiary amine (**e**), forming a zwitterion intermediate (**f**). By the traditional carbamate mechanism, a proton is then transferred to another mole of the amine (Scheme 1). However in the PIL, there are several species that are possible acceptors of this proton. As a transition state, the carbamate must initially form zwitterionic species (**f**), which could not be located on the calculated potential energy surface (PES) of these species. In our theoretical calculations, two cations and two anions were used to represent the PIL bulk and multiple relaxed scans did not produce a maximum on the PES for the CO_2 addition. Moreover, the intermediate zwitterion species was found to easily donate the proton to the nearby formate/acetate anion during the actual simulations as shown in Scheme 2. This suggests that the competition for the carbamate proton between the PIL cation and the anion, is shifted towards the anion. The intermolecular transfer of the proton from the N atom to the oxygen centre on the zwitterion (**h**) was also investigated. Based on the total electronic energies the formation of neutral acid (**d**) over the intermolecular proton transfer (**h**) was favoured by 5.7 kJ mol^{-1} for formate and 38.0 kJ mol^{-1} for acetate, suggesting that the transfer to the anion was more likely. This is an unexpected result on the basis of aqueous pK_a^{aq} values – since the PIL cation is distinctly more basic ($pK_a^{aq} \approx 6$) than acetate ($pK_a^{aq} \approx 4.8$) in water. It obviously further supports the argument that one needs to be careful when predicting proton transfer in PILs based on acidity/basicity measure in aqueous solution. However, as discussed above, such deviations from aqueous behavior in neat PILs is commonly observed,[6] particularly when tertiary amine sites are involved.

In order to investigate this further, computational techniques were used to produce the IR spectra of both PILs with carbamate functionality (**g**, **d**) (structures are shown in Fig. S4, ESI†). A comparison of the predicted vibrations to the experimental spectrum of CO_2 loaded PILs are shown in Fig. 6a for DMEDAH formate and Fig. 6b for DMEDAH acetate.

In Fig. 6a the neat DMEDAH formate is shown in blue, while the sample loaded at 1 atm CO_2 is shown in green. Shown in red is the computationally generated FTIR spectrum of the calculated cluster of DMEDAH formate containing the carbamate moiety on the primary amine of DMEDAH. The predicted spectrum was scaled by 0.933 to the experimental C–H stretch in formate assigned to 2773 cm^{-1}. The experimental data show several key changes between the neat sample and that loaded with CO_2. In particular, there is a significant change in the shape of the peaks located at around 1500 cm^{-1}, as well as the region between 1200–1300 cm^{-1}. These areas are indicative of the carbonyl region expected from the carbamate functionality that is formed upon CO_2 capture. Finally, a clear shoulder is developed at around 1650 cm^{-1}, which does not occur at all in the neat sample.

Based on the analysis of the predicted spectrum, several key bands were attributed to the formate anion and the formation of the carbamate. The bands at 1282 cm^{-1} and 1168 cm^{-1} that are attributed to the carbamate C–O stretch correlate to an increase in intensity of the experimental data, suggesting these

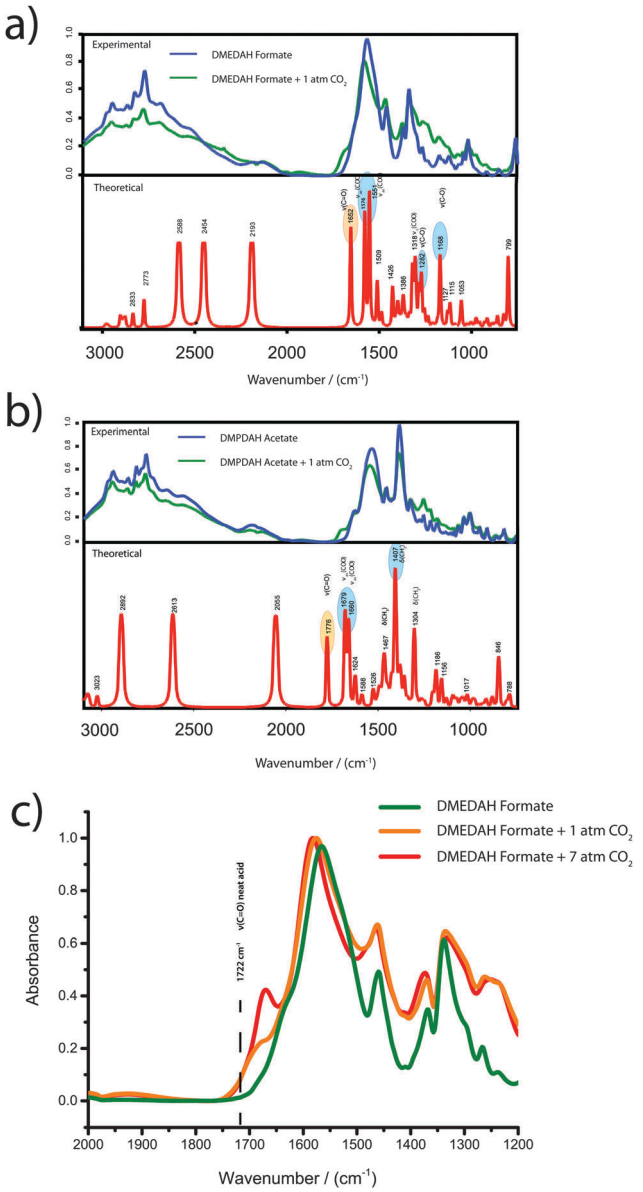

Fig. 6 (a) Experimental and theoretical spectra of DMEDAH formate with and without CO_2 loaded at 1 atmosphere (Fig. S4, ESI†). (b) Experimental spectra of DMPDAH acetate with and without CO_2 loaded at 1 atmosphere and Theoretical spectra of DMEDAH acetate loaded with CO_2 (Fig. S4, ESI†) (c) experimental ATR-IR spectra of DMEDAH formate under different loading conditions.

peaks are indeed present underneath the surrounding bands. The C═O stretch in the carbamate was calculated to be at 1576 cm^{-1}, which is in good agreement with the broad peak at 1500 cm^{-1} in the experimental spectrum. Importantly, a clear band at 1662 cm^{-1} of the calculated spectra is proposed to be responsible for the shoulder seen at around 1700 cm^{-1} in the experimental spectrum. This band is attributed to the ν(C═O) of the formic acid species of the calculated cluster (highlighted in orange), suggesting that the weak acid anion is indeed the terminal proton acceptor, and that **g** and **d** are present in the CO_2 loaded sample. The ν(C═O) stretching peak for pure formic acid is indicated on the spectrum – while it does not exactly align with that seen in the experimental data, it is not unexpected to see a deviation from the pure material when discussing a complex PIL matrix, which can shift peaks significantly depending on the local arrangement of anions and cations.

For the DMPDAH acetate PIL system (Fig. 6b) it is clear that the magnitude of the observed changes in the experimental spectra are less significant than for the DMEDAH formate system, with the key changes arising from higher intensity in the fingerprint region of the spectrum. A scaling factor of 0.997 was used to fit the predicted spectrum to reproduce the C–C stretch of the acetate observed at 1392 cm^{-1} in the experimental spectrum. Similarly to the formate case, a shoulder is seen to develop at around 1700 cm^{-1}, which aligns well with the ν(C═O) stretching vibration observed in the calculated spectra of the acetic acid. This clearly suggests the formation of the neutral acid in the system.

These observations for both the formate and acetate systems suggest that these PILs should be able to achieve a theoretical limit of 1 mole CO_2 per mole amine, as the anion becomes involved as the terminal proton acceptor. This hypothesis is supported by the fact that in the presence of a much less basic counter-anion such as NTf_2, the CO_2 uptake is drastically reduced (Table 1), most likely due to the inability of the basic NTf_2 anion to accept this proton to form the free acid. While uptake values in excess of 0.5 mol/mol have been observed here, the values remain significantly lower than 1 : 1. It is believed that the increasing viscosity upon CO_2 addition and low CO_2 pressure may be responsible for the slow kinetics/diffusion and hence, smaller than expected uptake.

In order to test whether the neutral acid concentration would increase with an increase in the CO_2 content, the DMEDAH formate sample was subjected to an elevated CO_2 pressure (Fig. 6c). After return to atmospheric CO_2 conditions, an increase in CO_2 related features can be also be seen in Fig. 6c, where the formic acid peak has significantly increased in intensity with the increase in CO_2 partial pressure (full details are described in the ESI,† and Fig. S5). While this supports the acid formation mechanism that provides a higher theoretical capacity, it would appear that it is not strongly favored, even under elevated CO_2 pressures. It should also be noted that there is undoubtedly a proportion of this increase that must be attributed to increased physical absorption of CO_2. In short, the spectroscopic and computational results suggest that the weak carboxylate acid is the terminal proton acceptor can facilitate an uptake ratio >0.5 mol/mol in these PIL systems.

4 Conclusions

The uptake of CO_2 by DMEDAH formate and DMPDAH acetate PILs has been found to be achievable at ambient temperature and regeneration can be carried out at temperatures as low as 40 °C. These diamine PILs were shown to be capable of repeated CO_2 capture/regeneration cycles using a DSC based method. The enthalpy of desorption cycle was found to be

40 kJ mol^{-1} and 50 kJ mol^{-1} for DMEDAH formate and DMPDAH acetate, respectively. Spectroscopic evidence suggests that the terminal proton acceptor after the initial zwitterion formation can, to some equilibrium extent, be the carboxylate anion that is part of the PIL, allowing access to $n(CO_2)/n$(amine) uptakes greater than 0.5. We conclude that both DMEDAH formate and DMPDAH acetate show excellent potential for CO_2 scrubbing in sealed atmospheres under ambient conditions and should be considered for further study to overcome the limitation of high viscosity.

Acknowledgements

DRM would like to acknowledge the Australian Research Council (ARC) for his Australian Laureate Fellowship. EII would like to acknowledge the ARC for her Future Fellowship and the National Computational Infrastructure (NCI) and the Monash *e*Research Centre for generous allocation of computer time. The authors would also like to thank Dr Peter Nichols for his assistance with the ^{13}C NMR experiments, Dr Finlay Shanks for his assistance with the ATR-IR experiments and Dr Marc Marshal for the use of his autoclave.

References

1 D. M. D'Alessandro, B. Smit and J. R. Long, *Angew. Chem., Int. Ed.*, 2010, **49**, 6058–6082.
2 W. M. Budzianowski, *Int. J. Global Warm.*, 2015, **7**, 184–225.
3 S. Choi, J. H. Drese and C. W. Jones, *ChemSusChem*, 2009, **2**, 796–854.
4 A. Guais, G. Brand, L. Jacquot, M. Karrer, S. Dukan, G. Grévillot, T. J. Molina, J. Bonte, M. Regnier and L. Schwartz, *Chem. Res. Toxicol.*, 2011, **24**, 2061–2070.
5 R. D. Rogers and K. R. Seddon, *Science*, 2003, **302**, 792–793.
6 J. Stoimenovski, E. I. Izgorodina and D. R. MacFarlane, *Phys. Chem. Chem. Phys.*, 2010, **12**, 10341–10347.
7 M. Yoshizawa, W. Xu and C. A. Angell, *J. Am. Chem. Soc.*, 2003, **125**, 15411–15419.
8 M. S. Miran, H. Kinoshita, T. Yasuda, M. A. B. H. Susan, K. Dokko and M. Watanabe, *Mater. Res. Soc. Symp. Proc.*, 2012, **1473**, 1–6.
9 H. Zhang, Y. Zhou and X. Song, *Prog. Chem.*, 2015, **27**, 174–191.
10 M. P. Gimeno, M. C. Mayoral and J. M. Andrés, *Energy Fuels*, 2013, **27**, 3928–3935.
11 D. Nan, J. Liu and W. Ma, *Chem. Eng. J.*, 2015, **276**, 44–50.
12 G. Léonard, D. Toye and G. Heyen, *Int. J. Greenhouse Gas Control*, 2014, **30**, 171–178.
13 S. Seo, M. A. DeSilva and J. F. Brennecke, *J. Phys. Chem. B*, 2014, **118**, 14870–14879.
14 I. Niedermaier, M. Bahlmann, C. Papp, C. Kolbeck, W. Wei, S. Krick Calderón, M. Grabau, P. S. Schulz, P. Wasserscheid, H.-P. Steinrück and F. Maier, *J. Am. Chem. Soc.*, 2014, **136**, 436–441.
15 R. Vijayaraghavan, S. J. Pas, E. I. Izgorodina and D. R. MacFarlane, *Phys. Chem. Chem. Phys.*, 2013, **15**, 19994–19999.
16 M. J. Frisch, G. W. Trucks, H. B. Schlegel, G. E. Scuseria, M. A. Robb, J. R. Cheeseman, G. Scalmani, V. Barone, B. Mennucci, G. A. Petersson, H. Nakatsuji, M. Caricato, A. F. Izmaylov, J. Bloino, G. Zheng, J. L. Sonnenberg, M. Hada, M. Ehara, K. Toyota and R. Fukuda, *Gaussian 09, Revision B*, Gaussian, Inc., Wallingford, CT, 2009.
17 Y. Zhao and D. G. Truhlar, *Theor. Chem. Acc.*, 2008, **120**, 215–241.
18 R. A. Kendall, T. H. Dunning Jr and R. J. Harrison, *J. Chem. Phys.*, 1992, **96**, 6796–6806.
19 S. Zahn, D. R. Macfarlane and E. I. Izgorodina, *Phys. Chem. Chem. Phys.*, 2013, **15**, 13664–13675.
20 M. Cossi, N. Rega, G. Scalmani and V. Barone, *J. Comput. Chem.*, 2003, **24**, 669–681.
21 A. S. R. Chesman, J. L. Hodgson, E. I. Izgorodina, A. Urbatsch, D. R. Turner, G. B. Deacon and S. R. Batten, *Cryst. Growth Des.*, 2014, **14**, 1922–1932.
22 C. Mathonat, V. Majer, A. E. Mather and J. P. E. Grolier, *Ind. Eng. Chem. Res.*, 1998, **37**, 4136–4141.
23 L. E. Ficke and J. F. Brennecke, *J. Phys. Chem. B*, 2010, **114**, 10496–10501.
24 M. Massel, A. L. Revelli, E. Paharik, M. Rauh, L. O. Mark and J. F. Brennecke, *J. Chem. Eng. Data*, 2015, **60**, 65–73.
25 K. A. Mumford, S. J. Pas, T. Linseisen, T. M. Statham, N. Johann Nicholas, A. Lee, K. Kezia, R. Vijayaraghavan, D. R. MacFarlane and G. W. Stevens, *Int. J. Greenhouse Gas Control*, 2015, **32**, 129–134.
26 N. M. Rocher, E. I. Izgorodina, T. Rüther, M. Forsyth, D. R. MacFarlane, T. Rodopoulos, M. D. Horne and A. M. Bond, *Chem. – Eur. J.*, 2009, **15**, 3435–3447.
27 E. I. Izgorodina, J. L. Hodgson, D. C. Weis, S. J. Pas and D. R. MacFarlane, *J. Phys. Chem. B*, 2015, **119**, 11748–11759.